NeuroImage: Clinical 31 (2021) 102687

Contents lists available at ScienceDirect

NeuroImage: Clinical

journal homepage: www.elsevier.com/locate/ynicl

FDG-PET in presymptomatic *C9orf72* mutation carriers

Karteek Popuri [a], Mirza Faisal Beg [a], Hyunwoo Lee [b], Rakesh Balachandar [a], Lei Wang [c], Vesna Sossi [d], Claudia Jacova [e], Matt Baker [f], Elham Shahinfard [d], Rosa Rademakers [f], Ian R. A. Mackenzie [g], Ging-Yuek R. Hsiung [b,*]

[a] *School of Engineering Science, Simon Fraser University*
[b] *Division of Neurology, Department of Medicine, University of British Columbia*
[c] *Departments of Psychiatry and Behavioral Sciences and Radiology, Feinberg School of Medicine, Northwestern University*
[d] *Department of Physics and Astronomy, University of British Columbia*
[e] *School of Graduate Psychology, Pacific University*
[f] *Department of Neuroscience, Mayo Clinic*
[g] *Department of Pathology and Laboratory Medicine, University of British Columbia*

A B S T R A C T

Objective: Our aim is to investigate patterns of brain glucose metabolism using fluorodeoxyglucose positron emission tomography (FDG-PET) in presymptomatic carriers of the *C9orf72* repeat expansion to better understand the early preclinical stages of frontotemporal dementia (FTD).
Methods: Structural MRI and FDG-PET were performed on clinically asymptomatic members of families with FTD caused by the *C9orf72* repeat expansion (15 presymptomatic mutation carriers, *C9orf72*+; 20 non-carriers, *C9orf72*-). Regional glucose metabolism in cerebral and cerebellar gray matter was compared between groups.
Results: The mean age of the *C9orf72*+ and *C9orf72*- groups were 45.3 ± 10.6 and 56.0 ± 11.0 years respectively, and the mean age of FTD onset in their families was 56 ± 7 years. Compared to non-carrier controls, the *C9orf72*+ group exhibited regional hypometabolism, primarily involving the cingulate gyrus, frontal and temporal neocortices (left > right) and bilateral thalami.
Conclusions: The *C9orf72* repeat expansion is associated with changes in brain glucose metabolism that are demonstrable up to 10 years prior to symptom onset and before changes in gray matter volume become significant. These findings indicate that FDG-PET may be a particularly sensitive and useful method for investigating and monitoring the earliest stages of FTD in individuals with this underlying genetic basis.

1. Introduction

Frontotemporal dementia (FTD) is a heterogeneous clinical syndrome, presenting with changes in behavior, personality, language and motor function. (Woollacott and Rohrer, 2016) A family history is reported in over 40% of FTD cases, with microtubule associated protein tau (*MAPT*) and granulin (*GRN*) mutations and abnormal repeat expansion in the chromosome 9 open reading frame 72 (*C9orf72*) gene responsible for the majority of inherited FTD. (Pottier et al., 2016) Although the clinical features of symptomatic FTD have been well characterized, little is known about the earliest stages of disease when therapeutic intervention is most likely to be beneficial. A better understanding of the early natural history of FTD, combined with the development of biomarkers to enable earlier diagnosis, track disease progression and monitor the effects of treatment are urgently needed. (Meeter et al., 2017; Tsai and Boxer, 2016) Individuals from families with inherited FTD provide a unique opportunity to investigate these important issues because they have a predictable risk for developing the disease. (Rohrer et al., 2013)

Many studies have demonstrated structural and functional neuroimaging changes in fully affected FTD patients, with specific patterns of abnormality correlating with both the clinical presentation and/or the underlying genetic cause. (Gordon et al., 2016; Whitwell et al., 2012) Fewer studies have investigated the imaging features of the preclinical stage of FTD; however, several have shown that carriers of FTD-causing mutations may exhibit changes several years (even decades) prior to symptom onset. (Alexander et al., 2018; Cash et al., 2018; Floeter et al., 2018; Jacova et al., 2013; Papma et al., 2017; Popuri et al., 2018; Rohrer et al., 2015) Since models of neurodegenerative disease predict neuronal dysfunction to be an early change that precedes neuronal death, brain atrophy and clinical manifestations, techniques that evaluate changes reflective of neuronal dysfunction may be particularly useful for

* Corresponding author.
E-mail address: hsiung@mail.ubc.ca (G.-Y.R. Hsiung).

https://doi.org/10.1016/j.nicl.2021.102687
Received 26 August 2020; Received in revised form 19 April 2021; Accepted 20 April 2021
Available online 25 April 2021

investigating the initial stages of disease. (Rohrer et al., 2013; Morbelli et al., 2016) For example, reduced 18F-fluorodeoxyglucose positron emission tomography (FDG-PET) signal can be detected earlier than structural magnetic resonance imaging (MRI) changes in presymptomatic carriers of *GRN* (Jacova et al., 2013; Caroppo et al., 2015) or *MAPT* (Deters et al., 2014) mutations. This suggests that reduced brain glucose metabolism associated with factors such as neuropil and synaptic abnormalities, (Ou et al., 2019) altered astrocyte activity, (Zimmer et al., 2017) or blood-brain-barrier dysfunction (Sweeney et al., 2018) may precede the manifestation of neuroaxonal degeneration as reflected in structural atrophy.

To better understand the presence of metabolic alterations during the preclinical stages of FTD due to genetic cause, we used FDG-PET to evaluate brain glucose uptake patterns in clinically asymptomatic participants with the *C9orf72* repeat expansion.

2. Methods

2.1. Participants

Study participants were recruited through the University of British Columbia (UBC) hospital clinic for Alzheimer's disease and related disorders. All were members of families with FTD caused by the *C9orf72* repeat expansion and all were considered to be at-risk for FTD by virtue of having a first-degree relative who was either fully affected or known to carry the mutation (or both). Throughout the study, participants remained blinded to their genetic mutation status, as did the researchers performing the clinical assessments and the subsequent image analysis. Detailed neurological examination and cognitive testing, including Mini Mental State Examination (MMSE), Frontal Assessment Battery (FAB), and Frontal Behavioral Inventory (FBI), manual muscle test (MRC motor rating), Amyotrophic Lateral Sclerosis Functional Rating scale – revised (ALS-FRS-R), determined that none of the participants fulfilled diagnostic criteria for possible or probable behavioral variant FTD (bvFTD), (Rascovsky et al., 2011) primary progressive aphasia (PPA), (Gorno-Tempini et al., 2011) or amyotrophic lateral sclerosis (ALS), (Brooks et al., 2000) and all were free from any neurological or cognitive deficit; therefore, all were classified as being asymptomatic. Detailed demographic and clinical information is presented in table 1. Years prior to expected FTD onset was calculated by subtracting the participant's age at the time of their PET scan from the mean age of disease onset within their family.

3. Standard protocol approvals, registrations and consents

The study was reviewed by the UBC research ethics board and each participant provided written informed consent.

4. Genetic status

DNA extracted from peripheral blood was used for genetic analysis at the Mayo Clinic, Jacksonville, Florida, using standard protocols. (Baker et al., 2006; DeJesus-Hernandez et al., 2011) Participants were screened for the *C9orf72* repeat expansion and each was classified as being a mutation carrier (*C9orf72*+) or non-carrier (*C9orf72*-).

5. Image acquisition

Structural MRI scans were obtained on a 1.5T GE Signa scanner (GE Medical Systems, Milwaukee, WI). A T1-weighted 3D MRI was acquired with echo time of 4.8 ms, repetition time of 10.3 ms, inversion time of 450 ms, field of view of 25 cm, matrix size 256 x 256 and 170 contiguous 1.0 mm thick slices.

FDG-PET scans were acquired using the high-resolution research tomograph (HRRT-Siemens/CTI, Knoxville, TN). Data were acquired in list mode starting 30 minutes after injection of 5mCi of FDG and framed into six frames (each 5-minutes apart) prior to reconstruction with the ordinary Poisson expectation maximization algorithm, and corrected for detector normalization, dead time, scatter, and attenuation. The images were spatially realigned with rigid-body transformation to minimize the impact of motion artifacts during scans. The realigned images were averaged to obtain a single time-integrated 3D PET image with isotropic 1.2 mm^3 voxels storing the raw FDG uptake values (Bq/ml/min).

Table 1
Demographic and clinical features of participants.

	C9orf72+	*C9orf72*-	*p*
number	15	20	-
age (years) [range]	45.3 ± 10.6 (Fischl et al., 2002; Herholz et al., 1990, 2002; Sanabria-Diaz et al., 2013; Ihaka and Gentleman, 1996; Benjamini and Hochberg, 1995; Rutherford et al., 2012; De Vocht et al., 2020; Mutsaerts et al., 2019; Bertrand et al., 2018; Lee et al., 2017; Walhout et al., 2015; Boeve et al., 2012; Cistaro et al., 2014; Josephs et al., 2014; Kerklaan et al., 2014; McDade et al., 2012; Van Laere et al., 2014)	56.0 ± 11.0[34–65]	**0.0066**
sex(male: female)	8:7	12:8	0.6933
handedness (right:left)	12:3	20:0	**0.0365**
education (years)	14 ± 3	13 ± 3	0.5051[a]
MMSE score [range]	29 ± 1 (Desikan et al., 2006; Fischl et al., 2002; Herholz et al., 1990, 2002)	29± 1 (Dale et al., 1999; Desikan et al., 2006; Fischl et al., 2002; Herholz et al., 1990, 2002)	0.2883[a]
FAB score [range]	17 ± 2 (Jacova et al., 2013; Papma et al., 2017; Popuri et al., 2018; Rohrer et al., 2015; Morbelli et al., 2016; Caroppo et al., 2015; Deters et al., 2014; Ou et al., 2019)	16 ± 2 (Popuri et al., 2018; Rohrer et al., 2015; Morbelli et al., 2016; Caroppo et al., 2015; Deters et al., 2014; Ou et al., 2019)	0.1655[a]
FBI score [range]	1 ± 1[0–4]	0 ± 1[0–4]	0.7943[a]
Manual Muscle Testing	100 ± 0.2[98–100]	100 ± 0.1[99–100]	0.8241[a]
ALS-FRS-R	19.4 ± 0.6 (Zimmer et al., 2017; Sweeney et al., 2018)	19. 6 ± 0.4 (Zimmer et al., 2017; Sweeney et al., 2018)	0.7792[a]
mean age FTD onset in family (years)	56 ± 9	56 ± 6	0.8806
years to mean age of FTD onset	11 ± 11	0 ± 10	**0.0066**

C9orf72+, *C9orf72* mutation carrier; *C9orf72*-, non-carrier member of family with *C9orf72* mutation; FAB, Frontal Assessment Battery (maximum score = 18); FBI, Frontal Behavioral Inventory (maximum score = 72); MMSE, Mini Mental State Exam (maximum score = 30); ALS-FRS-R, Amyotrophic Lateral Sclerosis – Functional Rating Scale - revised

[a] Data did not follow normal distribution; therefore, non-parametric test (Wilcoxon rank sum) was employed.

6. MRI parcellation into cortical and subcortical ROIs

T1 MRI images were initially segmented into gray matter (GM), white matter (WM) and cerebrospinal fluid (CSF) tissue regions (Dale

et al., 1999) using the FreeSurfer 5.3 software package (https://surfer.nmr.mgh.harvard.edu). Briefly, the FreeSurfer processing pipeline consisted of the following steps: 1) affine registration of T1 MRI image to the MNI305 space, 2) B1 bias field correction, 3) non-rigid registration to the MNI305 space, and 4) atlas-based structure labeling based on the maximum likelihood of the probability atlas. The automated tissue segmentations were visually inspected and a rigorous quality control procedure was employed to manually correct the identified errors following FreeSurfer's troubleshooting guidelines. Subsequently, FreeSurfer's cortical (Desikan et al., 2006) and subcortical (Fischl et al., 2002) labeling pipelines were used to obtain a parcellation of the GM tissue region into 85 different anatomical regions of interest (ROIs).

7. ROI-wise FDG SUVR measures

For each participant, a 12 degrees of freedom (DOF) transformation was estimated between the MRI image and the corresponding FDG-PET image using the intermodal linear registration facility available as part of the FSL FLIRT program (https://fsl.fmrib.ox.ac.uk/fsl/fslwiki/FLIRT). This transformation matrix was then used to resample the anatomical ROIs in the T1 MRI space to the PET space. All registrations were visually checked and confirmed. The ratio of the mean FDG-PET concentration in a given ROI to that of the brainstem (reference ROI with no difference between groups) was taken as the standardized uptake value ratio (SUVR) of that particular ROI. (Herholz et al., 1990, 2002; Sanabria-Diaz et al., 2013) A total of 84 SUVR measurements were obtained for each individual.

7.1. Statistical analysis

The R statistical package (www.r-project.org) (Ihaka and Gentleman, 1996) was used to compare demographic and clinical variables between groups. Normality of the data was checked using Shapiro-Wilk test following which group differences were determined using *t*-test for parametric data (normal distribution) and Wilcoxon test for non-parametric data. Chi-square test was used for comparing the sex and handedness distributions between the groups. Results were considered significant at $p<0.05$.

ROI-wise group differences in the FDG-PET SUVR measures were examined using two separate generalized linear models (GLMs), fitted using the R lm package that assumes Gaussian error distribution. The first model used the mean SUVR (i.e. sum of the SUVR divided by the ROI volume), adjusting for sex, handedness, difference in age at the time of obtaining PET and years prior to expected FTD onset. The second model used the sum SUVR (i.e. sum of the SUVR), adjusting for the same covariates used in Model 1 plus the GM ROI volume to account for the expected influence of the ROI size. In summary, the models were as follows:

Model 1: **mean_SUVR** = 1 + age + sex + time to onset + handedness

Model 2: **sum_SUVR** = 1 + age + sex + time to onset + handedness + **GM_volume**

Significance levels were adjusted for multiple comparisons using the false discovery rate (FDR) approach by Benjamini & Hochberg (Benjamini and Hochberg, 1995), with the significance threshold set at $p<0.05$.

8. Data availability

Deidentified clinical, imaging, and molecular data will be made available at the Canadian Association of Research Library (http://www.carl-abrc.ca/).

9. Results

9.1. Demographic and clinical data

The baseline demographic and clinical information of the participants are shown in Table 1. The *C9orf72*+ group was significantly younger (45.3 ± 10.6 years) than the *C9orf72*- group (56.0 ± 11.0 years) (p=0.007). Left handed participants were only present in the *C9orf72*+ group, representing 20% (p<0.05). Otherwise, the groups were similar with regards to sex, education, and other clinical cognitive assessment scores.

10. Gray matter volume measures

Comparisons of the ROIs did not show any significant difference in gray matter volume between the *C9orf72*+ and the *C9orf72*- groups when age, sex, handedness, and estimated time to onset were included as covariates (Table 2).

11. FDG-PET SUVR measures

Participants in the *C9orf72*+ group showed significant hypometabolism in multiple brain regions compared to the *C9orf72*- group, with more widespread involvement of the left hemisphere (Table 2). To account for potential influence of GM volume differences on PET-SUVR measures, we used two models to compare the difference in regional FDG tracer activities. There were more statistically significant differences in FDG uptake in the ROIs with Model 2. The brain regions primarily involved included multiple frontal lobe areas, the cingulate gyrus, precuneus, left pre- and postcentral gyri, left superior temporal gyrus, right inferior temporal gyrus and the thalamus bilaterally (Figure 1). There was no correlation between the age of the participants and the extent of FDG-PET abnormality; in fact, it was the younger *C9orf72* mutation carriers who had the greatest number of ROIs with reduced uptake and the ROIs with the most severe hypometabolism.

12. Discussion

Since the *C9orf72* repeat expansion causes disease with an autosomal dominant pattern of inheritance with very high penetrance, (Pottier et al., 2016) asymptomatic mutation carriers can be considered to be in a preclinical stage of disease. (Rohrer et al., 2013) Furthermore, the size of the pathogenic *C9orf72* repeat expansion does not seem to influence its phenotypic expression; therefore, the *C9orf72*+ individuals can be considered genetically homogeneous. (Rutherford et al., 2012) Characterization of the longitudinal change in early disease stage is essential to better understand the natural history of disease and to develop rational clinical endpoints for therapeutic trials. Our current findings demonstrate that FDG-PET hypometabolism is detectable in asymptomatic *C9orf72* mutation carriers on average up to 10 years prior to onset of dementia.

To date, few studies have investigated preclinical FTD subjects with FDG-PET. A recent study of presymptomatic *C9orf72* carriers also found significant hypometabolism in the insular cortices, central opercular cortex, basal ganglia, and thalami compared to healthy controls, that preceded any significant elevation of neurofilament levels. (De Vocht et al., 2020) These regions were consistent with our findings, although we additionally showed significant hypometabolism in the inferior parietal lobe and the adjacent regions such as the posterior and isthmus cingulate gyri. In particular, the parietal involvement was also shown in a perfusion MRI-based study of presymptomatic *C9orf72* carriers. (Mutsaerts et al., 2019) These findings highlight that our findings are consistent with that study, showing significant hypometabolism in similar regions of the brain, despite the fact that *C9orf72* patients have a high heterogeneity in their eventual clinical presentation, which may include bvFTD, progressive aphasias, and motor neuron disease. The

Table 2
FDG-PET SUVR values and group difference t statistics (*C9orf72+* vs. *C9orf72-*) in each ROI

	Mean SUVR ± SD						**Sum SUVR (GM vol covar) ± SD**					
	Left			**Right**			**Left**			**Right**		
	C9+	**C9-**	**t-stat**	**C9+**	**C9-**	**t-stat**	**C9+**	**C9-**	**t-stat**	**C9+**	**C9-**	**t-stat**
Frontal pole	1.66 ± 0.16	1.72 ± 0.16	-2.10	1.66 ± 0.16	1.73 ± 0.17	-2.42	732.72 ± 173.45	740.54 ± 152.46	-1.06	**993.01 ± 196.00**	**1022.22 ± 207.35**	**-2.55***
Pars opercularis	**1.79 ± 0.11**	**1.88 ± 0.18**	**-3.31***	1.82 ± 0.10	1.91 ± 0.20	-2.26	**4675.83 ± 629.21**	**4581.83 ± 943.13**	**-3.14***	4131.86 ± 962.80	4082.11 ± 881.07	-2.06
Pars orbitalis	1.61 ± 0.09	1.66 ± 0.17	-1.84	1.62 ± 0.15	1.68 ± 0.15	-1.37	2017.48 ± 406.30	1926.05 ± 387.38	-1.33	2283.58 ± 469.45	2311.23 ± 407.68	-1.26
Pars triangularis	1.69 ± 0.13	1.77 ± 0.18	-2.17	1.66 ± 0.14	1.78 ± 0.21	-2.14	2943.56 ± 554.03	3127.25 ± 406.25	-2.02	3431.35 ± 697.65	3727.17 ± 580.72	-2.24
Lateral orbitofrontal	1.67 ± 0.11	1.72 ± 0.16	-1.65	1.67 ± 0.11	1.72 ± 0.15	-1.51	6921.14 ± 1015.84	6873.53 ± 1203.03	-1.30	6722.43 ± 1060.16	6722.14 ± 1069.96	-1.39
Medial orbitofrontal	1.56 ± 0.12	1.61 ± 0.17	-1.85	1.59 ± 0.12	1.64 ± 0.16	-1.66	4454.22 ± 760.00	4558.61 ± 931.31	-1.47	4595.80 ± 694.84	4342.46 ± 660.13	-0.76
Superior frontal	**1.71 ± 0.10**	**1.80 ± 0.15**	**-3.59***	1.72 ± 0.11	1.81 ± 0.16	-3.17	**19073.42 ± 2562.14**	**19856.42 ± 3074.87**	**-3.01***	**19117.75 ± 2509.43**	**19855.68 ± 2861.57**	**-3.03***
Rostral middle frontal	**1.81 ± 0.13**	**1.96 ± 0.17**	**-3.75***	1.85 ± 0.14	1.96 ± 0.18	-2.64	**14352.34 ± 2890.53**	**15251.27 ± 3106.07**	**-3.44***	15162.95 ± 2791.87	15775.48 ± 2967.70	-2.17
Caudal middle frontal	**1.83 ± 0.14**	**1.94 ± 0.17**	**-4.07***	**1.82 ± 0.14**	**1.94 ± 0.20**	**-3.91***	**6434.53 ± 1254.40**	**6326.12 ± 1285.32**	**-3.61***	**5736.71 ± 1341.70**	**5685.74 ± 1182.96**	**-4.32***
Precentral	1.65 ± 0.10	1.74 ± 0.14	-3.36	1.66 ± 0.10	1.77 ± 0.16	-2.96	**10907.33 ± 1804.80**	**11650.18 ± 1765.39**	**-2.76***	**11357.71 ± 1925.17**	**11698.84 ± 1818.52**	**-2.79***
Paracentral	**1.61 ± 0.11**	**1.72 ± 0.13**	**-4.02***	1.63 ± 0.10	1.75 ± 0.15	-3.72	**2868.40 ± 364.48**	**2906.29 ± 536.33**	**-4.43***	**3193.79 ± 516.48**	**3384.85 ± 574.70**	**-3.77***
Postcentral	**1.55 ± 0.11**	**1.65 ± 0.13**	**-4.26***	1.58 ± 0.09	1.68 ± 0.16	-3.66	**7663.88 ± 1190.04**	**8171.40 ± 1589.19**	**-3.74***	**7586.28 ± 1000.05**	**7826.03 ± 1213.93**	**-3.04***
Superior parietal	1.54 ± 0.10	1.63 ± 0.18	-2.50	1.54 ± 0.10	1.65 ± 0.17	-2.72	9515.02 ± 1553.47	10410.96 ± 2085.96	-1.93	9960.31 ± 1704.84	10731.19 ± 1975.00	-2.27
Inferior parietal	1.65 ± 0.12	1.78 ± 0.17	-3.23	1.70 ± 0.12	1.83 ± 0.17	-3.25	**9791.99 ± 1380.92**	**11037.18 ± 1903.77**	**-2.52***	**12637.50 ± 2177.20**	**13902.85 ± 2384.63**	**-2.55***
Precuneus	**1.79 ± 0.13**	**1.92 ± 0.17**	**-3.53***	**1.78 ± 0.13**	**1.91 ± 0.16**	**-3.75***	**8544.59 ± 1285.09**	**8956.74 ± 1752.27**	**-2.83***	**8891.86 ± 1445.62**	**9183.66 ± 1718.60**	**-3.13***
Supramarginal	1.63 ± 0.14	1.73 ± 0.18	-2.82	1.66 ± 0.11	1.75 ± 0.16	-3.00	**9125.12 ± 1546.01**	**9219.17 ± 1466.40**	**-2.49***	**8838.80 ± 1511.14**	**9112.48 ± 1392.58**	**-2.46***
Insula	1.46 ± 0.07	1.51 ± 0.14	-2.46	1.45 ± 0.08	1.50 ± 0.13	-2.31	5281.41 ± 719.68	5629.58 ± 789.10	-1.72	5495.04 ± 737.85	5730.64 ± 793.13	-1.98
Rostral anterior cingulate	1.50 ± 0.13	1.55 ± 0.17	-1.69	1.44 ± 0.11	1.48 ± 0.16	-0.98	2385.29 ± 516.83	2288.96 ± 524.57	-1.41	1747.20 ± 363.56	1725.77 ± 369.77	-0.76
Caudal anterior cingulate	**1.49 ± 0.10**	**1.58 ± 0.16**	**-3.07***	1.51 ± 0.12	1.56 ± 0.16	-2.00	**1499.33 ± 513.80**	**1514.71 ± 481.96**	**-2.64***	**1777.39 ± 360.41**	**1566.35 ± 388.00**	**-2.50***
Posterior cingulate	**1.76 ± 0.13**	**1.87 ± 0.15**	**-3.62***	**1.77 ± 0.13**	**1.90 ± 0.15**	**-3.60***	**2732.62 ± 471.02**	**2846.58 ± 556.29**	**-3.21***	**2840.21 ± 527.82**	**2799.59 ± 600.39**	**-2.70***
Isthmus cingulate	**1.70 ± 0.15**	**1.82 ± 0.17**	**-2.90***	1.72 ± 0.14	1.86 ± 0.20	-2.85	**2249.94 ± 439.75**	**2240.34 ± 479.97**	**-2.46***	**2044.10 ± 404.09**	**2070.56 ± 437.32**	**-2.72***
Temporal pole	1.12 ± 0.07	1.12 ± 0.10	-1.61	1.09 ± 0.06	1.10 ± 0.09	-0.96	1687.66 ± 212.47	1540.42 ± 300.71	-0.35	1406.33 ± 206.02	1348.63 ± 281.54	-0.29
Bankssts	1.58 ± 0.13	1.68 ± 0.17	-2.39	1.63 ± 0.10	1.72 ± 0.19	-2.27	1939.36 ± 446.82	2149.16 ± 465.02	-2.27	1789.45 ± 503.62	2013.94 ± 371.92	-1.90
Superior temporal	**1.36 ± 0.08**	**1.44 ± 0.10**	**-4.03***	1.38 ± 0.07	1.46 ± 0.14	-2.55	**8416.27 ± 1659.27**	**8815.36 ± 1268.15**	**-3.44***	8629.36 ± 1287.44	8846.58 ± 1153.41	-2.24
Middle temporal	1.46 ± 0.10	1.57 ± 0.13	-3.38	1.44 ± 0.10	1.57 ± 0.14	-3.29	**7362.74 ± 1174.77**	**7624.53 ± 1392.01**	**-3.24***	**8783.32 ± 1272.46**	**8977.36 ± 1399.68**	**-3.10***
Inferior temporal	1.41 ± 0.09	1.51 ± 0.12	-3.19	**1.39 ± 0.07**	**1.50 ± 0.12**	**-3.95***	**8025.72 ± 1245.11**	**8544.01 ± 1592.34**	**-2.77***	**8305.74 ± 1749.54**	**8631.30 ± 1795.71**	**-3.85***
Transverse temporal	1.89 ± 0.15	1.99 ± 0.19	-1.79	1.89 ± 0.13	1.98 ± 0.22	-2.07	1164.88 ± 322.50	1172.89 ± 216.36	-1.91	904.32 ± 188.61	959.51 ± 224.57	-1.26
Fusiform	1.37 ± 0.09	1.44 ± 0.11	-2.58	1.39 ± 0.07	1.46 ± 0.10	-2.74	7504.81 ± 1628.73	7563.66 ± 1011.09	-2.34	**7251.84 ± 1187.70**	**7714.60 ± 801.49**	**-2.62***
Lingual	1.57 ± 0.10	1.65 ± 0.12	-2.52	1.59 ± 0.09	1.66 ± 0.15	-2.45	5260.26 ± 1214.82	5065.97 ± 740.52	-1.87	**5510.16 ± 1149.44**	**5339.03 ± 761.64**	**-2.46***
Entorhinal	1.07 ± 0.07	1.13 ± 0.09	-1.80	1.08 ± 0.07	1.15 ± 0.08	-2.41	1007.32 ± 223.04	984.49 ± 216.17	-1.47	856.23 ± 184.93	951.68 ± 179.36	-2.33
Parahippocampal	1.19 ± 0.07	1.24 ± 0.09	-2.31	1.20 ± 0.06	1.25 ± 0.10	-2.17	1477.19 ± 271.95	1482.89 ± 179.06	-1.97	1285.85 ± 187.60	1341.33 ± 177.36	-2.30
Pericalcarine	1.69 ± 0.12	1.76 ± 0.13	-1.67	1.73 ± 0.11	1.78 ± 0.15	-2.26	1797.83 ± 388.42	1800.99 ± 357.38	-1.64	2078.85 ± 358.07	2179.06 ± 424.37	-1.91
Lateral occipital	1.53 ± 0.11	1.63 ± 0.16	-2.42	1.55 ± 0.11	1.65 ± 0.16	-2.25	**8966.10 ± 1565.05**	**9377.97 ± 1387.26**	**-2.73***	**8843.14 ± 1793.12**	**9594.32 ± 1263.45**	**-2.45***
Cuneus	1.71 ± 0.15	1.80 ± 0.15	-2.42	1.69 ± 0.14	1.82 ± 0.16	-3.53	2384.87 ± 529.00	2561.58 ± 491.95	-1.63	**2549.63 ± 608.78**	**2908.56 ± 517.61**	**-3.22***
Accumbens	1.54 ± 0.10	1.60 ± 0.16	-0.58	1.51 ± 0.10	1.56 ± 0.10	-0.35	626.49 ± 98.59	586.10 ± 149.82	-0.59	600.38 ± 121.75	587.47 ± 130.54	-0.30
Hippocampus	1.09 ± 0.06	1.12 ± 0.07	-1.02	1.11 ± 0.06	1.14 ± 0.08	-0.82	2417.09 ± 307.69	2503.65 ± 233.08	-1.65	2635.40 ± 320.87	2629.25 ± 365.75	-0.58

(*continued on next page*)

Table 2 (*continued*)

	Mean SUVR ± SD						Sum SUVR (GM vol covar) ± SD					
	Left			Right			Left			Right		
	C9+	C9-	t-stat	C9+	C9-	t-stat	C9+	C9-	t-stat	C9+	C9-	t-stat
Amygdala	1.05 ± 0.05	1.05 ± 0.06	-0.42	1.08 ± 0.03	1.09 ± 0.07	-0.56	877.44 ± 129.57	867.44 ± 114.83	-0.45	917.67 ± 128.16	900.36 ± 127.59	-0.56
Thalamus	**1.30 ± 0.09**	**1.44 ± 0.07**	**-3.65***	**1.34 ± 0.08**	**1.51 ± 0.09**	**-3.54***	**5080.57 ± 590.94**	**5929.08 ± 734.94**	**-3.51***	**5010.13 ± 637.31**	**5787.37 ± 847.27**	**-3.19***
Pallidum	1.35 ± 0.10	1.45 ± 0.14	0.03	1.32 ± 0.09	1.38 ± 0.09	-0.07	1184.60 ± 179.61	1255.18 ± 268.82	0.38	1133.05 ± 137.82	1125.19 ± 166.39	-0.47
Putamen	1.76 ± 0.14	1.83 ± 0.11	-0.66	1.81 ± 0.14	1.90 ± 0.14	-0.31	5389.83 ± 796.09	5470.41 ± 912.67	-0.57	5082.51 ± 542.69	5328.46 ± 908.64	-0.18
Caudate	1.43 ± 0.14	1.48 ± 0.17	-1.06	1.47 ± 0.14	1.51 ± 0.17	-0.97	2863.77 ± 486.43	2905.96 ± 587.83	-0.89	3062.19 ± 442.27	3047.10 ± 568.53	-0.57
Cerebellum-cortex	1.26 ± 0.06	1.29 ± 0.08	-0.91	1.26 ± 0.06	1.29 ± 0.07	-1.11	34237.85 ± 3898.96	34551.46 ± 5907.94	-0.95	35821.36 ± 4067.46	36298.85 ± 6005.25	-1.04

*p<0.05 after false discovery rate correction (**Bold**)
GM volumes were not significantly different between *C9orf72*+ and *C9orf72*- in each ROI.

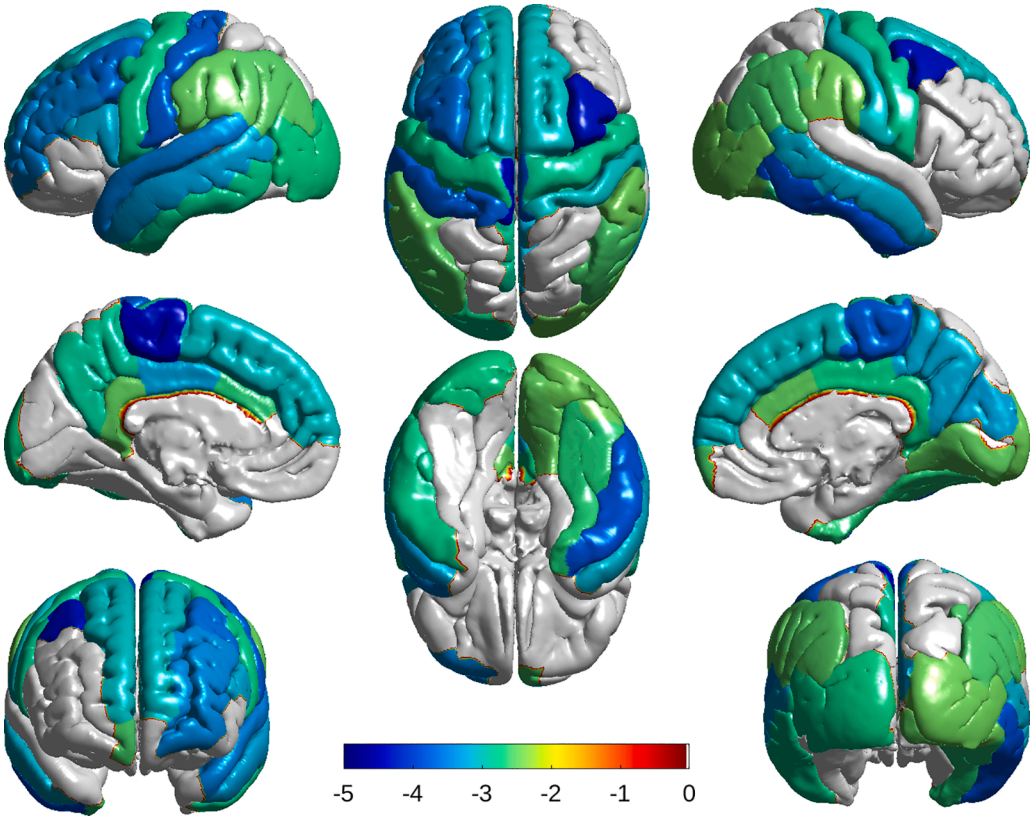

Fig. 1. Brain surface maps showing group differences in FDG-PET SUVR measures. Colored regions indicate significantly ($p < 0.05$) lower (towards blue) glucose uptake in mutation carriers compared to controls (corrected for age, sex, years prior to expected FTD onset and multiple comparisons). The *C9orf72* mutation carrier group (*C9orf72*+) showed anatomically widespread hypometabolism compared to non-carriers (*C9orf72*-), as well as significantly reduced uptake in the thalamus bilaterally (not shown).

FDG hypometabolism appears to be evident prior to any observable changes in clinical symptoms, suggesting that it may have utility as an early marker of disease activity, and as a method to assess the effect of any potential disease modifying therapy.

A number of other neuroimaging studies of asymptomatic *C9orf72* mutation carriers have used structural MRI and reported anatomically widespread cortical thinning, gray matter volume loss, reduced white matter integrity and reduced cerebral perfusion (Cash et al., 2018; Mutsaerts et al., 2019; Bertrand et al., 2018; Lee et al., 2017; Walhout et al., 2015; Papma et al., 2017; Popuri et al., 2018; Rohrer et al., 2015) may be evident up to 25 years prior to expected disease onset. (Rohrer et al., 2015) The wider variability in the specific anatomical regions reported to be involved may be due to the various imaging modalities employed among different studies or may reflect the heterogeneity in the eventual phenotype these individuals are predicted to develop. (Woollacott and Rohrer, 2016) Although we did not find significant differences in the gray matter ROI volumes in the present study, we have previously described regional cortical thinning in a slightly larger set of our presymptomatic *C9orf72* mutations carriers. This discrepancy is potentially attributable to the fact that a number of younger participants who participated in MRI imaging did not consent to PET due to concern about radiation exposure. (Popuri et al., 2018) As a result, the *C9orf72*- group was significantly older (on average by ~10 years) than the *C9orf72*+ group. The additional effect of aging-related structural changes in the *C9orf72*- group may have diminished the group differences in the GM volumes. Still, we found that the cortical brain regions involved, including the frontal, cingulate, precuneus, temporal region as well as the thalamus, overlap with our current findings in FDG-PET hypometabolism.

There have also been a few studies using FDG-PET to investigate fully affected *C9orf72* mutation carriers. (Boeve et al., 2012; Cistaro et al., 2014; Josephs et al., 2014; Kerklaan et al., 2014; McDade et al., 2012;

Van Laere et al., 2014) Most of these have involved small numbers of patients and the methods of analysis have varied, making it difficult to generalize the results. A report of five *C9orf72* mutation carriers who presented with bvFTD found bilateral reduced glucose metabolism that most consistently involved the anterior cingulate and frontal cortex;[40] whereas, a study of ALS patients found that those with the *C9orf72* mutation and sporadic cases both showed bifrontal hypometabolism; however, the mutation carriers had more widespread involvement that also included the cingulate, thalamus and precuneus. (Van Laere et al., 2014) Finally, a study that included 15 *C9orf72*+ ALS patients, 10 of whom also had FTD, reported symmetric hypometabolism in frontal cortex, cingulate, insula, caudate and thalamus, that was similar to sporadic ALS-FTD. (Cistaro et al., 2014) These studies suggest that the degree of clinical heterogeneity that exists, even among affected members of the same family who all carry the same pathogenic mutation, presents a major obstacle in the development of biomarkers and the design of clinical trials for FTD. (Woollacott and Rohrer, 2016; Tsai and Boxer, 2016)

As in most studies of rare genetic diseases, a major limitation of the current study is the limited sample size per group. This rendered it disadvantageous to perform voxel-wise comparisons, given that any error in high-dimensional registration to the standard template may particularly impact small-sample studies such as ours. To address this issue, we conducted group-wise comparisons based on the ROIs defined on the native-space MRIs using FreeSurfer. Still, despite the limited power associated with larger ROIs, we were able to demonstrate significant differences in regional brain glucose metabolism between *C9orf72*+ vs. *C9orf72*- participants. Another limitation is the cross-sectional analysis, which constrained our ability to make inferences about the rate of change. Additional longitudinal studies with FDG-PET will be important to further define the natural history of FTD, particularly the correlations between specific anatomical patterns of hypometabolism in the preclinical phase with the subsequent disease phenotype, as well as how changes in FDG uptake reflect disease progression.

In summary, we found that *C9orf72* mutations carriers who are at risk for developing FTD, demonstrate changes in brain glucose metabolism many years prior to the onset of symptoms. These findings suggest that FDG-PET is a useful technique for investigating and monitoring the earliest stages of disease. With potential antisense oligonucleotide and other disease modification therapy on the horizon, the ability to make early diagnosis and monitor disease progression will be extremely valuable for conduction of clinical trials. Future studies with larger samples and longitudinal follow up will be needed to fully characterize the natural history of progression into the clinical symptomatic phase in this disorder.

CRediT authorship contribution statement

Karteek Popuri: Data analysis, Initial drafting of the manuscript. **Mirza Faisal Beg and Vesna Sossi:** Study design, Data analysis, Manuscript revision. **Hyunwoo Lee:** Data analysis, Manuscript revision. **Rakesh Balachandar, Matt Baker, Elham Shahinfard, and Rosa Rademakers:** Data analysis. **Lei Wang and Claudia Jacova:** Study design. **Ian R.A. Mackenzie, Ging-Yuek, and R. Hsiung:** Study design, Data analysis, Funding acquisition, Supervision, and Manuscript revision.

References

Woollacott, I.O., Rohrer, J.D., 2016. The clinical spectrum of sporadic and familial forms of frontotemporal dementia. J Neurochem 138 (Suppl 1), 6–31.

Pottier, C., Ravenscroft, T.A., Sanchez-Contreras, M., Rademakers, R., 2016. Genetics of FTLD: overview and what else we can expect from genetic studies. J Neurochem 138 (Suppl 1), 32–53.

Meeter, L.H., Kaat, L.D., Rohrer, J.D., van Swieten, J.C., 2017. Imaging and fluid biomarkers in frontotemporal dementia. Nat Rev Neurol 13 (7), 406–419.

Tsai, R.M., Boxer, A.L., 2016. Therapy and clinical trials in frontotemporal dementia: past, present, and future. J Neurochem 138 (Suppl 1), 211–221.

Rohrer, J.D., Warren, J.D., Fox, N.C., Rossor, M.N., 2013. Presymptomatic studies in genetic frontotemporal dementia. Revue neurologique 169 (10), 820–824.

Gordon, E., Rohrer, J.D., Fox, N.C., 2016. Advances in neuroimaging in frontotemporal dementia. J Neurochem 138 (Suppl 1), 193–210.

Whitwell, J.L., Weigand, S.D., Boeve, B.F., et al., 2012. Neuroimaging signatures of frontotemporal dementia genetics: C9ORF72, tau, progranulin and sporadics. Brain 135 (Pt 3), 794–806.

Alexander, C., Zeithamova, D., Hsiung, G.R., Mackenzie, I.R., Jacova, C., 2018. Decreased Prefrontal Activation during Matrix Reasoning in Predementia Progranulin Mutation Carriers. J Alzheimers Dis 62 (2), 583–589.

Cash, D.M., Bocchetta, M., Thomas, D.L., et al., 2018. Patterns of gray matter atrophy in genetic frontotemporal dementia: results from the GENFI study. Neurobiol Aging 62, 191–196.

Floeter, M.K., Danielian, L.E., Braun, L.E., Wu, T., 2018. Longitudinal diffusion imaging across the C9orf72 clinical spectrum. J Neurol Neurosurg Psychiatry 89 (1), 53–60.

Jacova, C., Hsiung, G.Y., Tawankanjanachot, I., et al., 2013. Anterior brain glucose hypometabolism predates dementia in progranulin mutation carriers. Neurology 81 (15), 1322–1331.

Papma, J.M., Jiskoot, L.C., Panman, J.L., et al., 2017. Cognition and gray and white matter characteristics of presymptomatic C9orf72 repeat expansion. Neurology 89 (12), 1256–1264.

Popuri, K., Dowds, E., Beg, M.F., et al., 2018. Gray matter changes in asymptomatic C9orf72 and GRN mutation carriers. NeuroImage Clinical 18, 591–598.

Rohrer, J.D., Nicholas, J.M., Cash, D.M., et al., 2015. Presymptomatic cognitive and neuroanatomical changes in genetic frontotemporal dementia in the Genetic Frontotemporal dementia Initiative (GENFI) study: a cross-sectional analysis. Lancet Neurol 14 (3), 253–262.

Morbelli, S., Ferrara, M., Fiz, F., et al., 2016. Mapping brain morphological and functional conversion patterns in predementia late-onset bvFTD. European journal of nuclear medicine and molecular imaging 43 (7), 1337–1347.

Caroppo, P., Habert, M.O., Durrleman, S., et al., 2015. Lateral Temporal Lobe: An Early Imaging Marker of the Presymptomatic GRN Disease? J Alzheimers Dis 47 (3), 751–759.

Deters, K.D., Risacher, S.L., Farlow, M.R., et al., 2014. Cerebral hypometabolism and grey matter density in MAPT intron 10 +3 mutation carriers. Am J Neurodegener Dis 3 (3), 103–114.

Ou, Y.N., Xu, W., Li, J.Q., et al., 2019. FDG-PET as an independent biomarker for Alzheimer's biological diagnosis: a longitudinal study. Alzheimers Res Ther 11 (1), 57.

Zimmer, E.R., Parent, M.J., Souza, D.G., et al., 2017. [(18)F]FDG PET signal is driven by astroglial glutamate transport. Nat Neurosci 20 (3), 393–395.

Sweeney, M.D., Sagare, A.P., Zlokovic, B.V., 2018. Blood-brain barrier breakdown in Alzheimer disease and other neurodegenerative disorders. Nat Rev Neurol 14 (3), 133–150.

Rascovsky, K., Hodges, J.R., Knopman, D., et al., 2011. Sensitivity of revised diagnostic criteria for the behavioural variant of frontotemporal dementia. Brain 134 (Pt 9), 2456–2477.

Gorno-Tempini, M.L., Hillis, A.E., Weintraub, S., et al., 2011. Classification of primary progressive aphasia and its variants. Neurology 76 (11), 1006–1014.

Brooks, B.R., Miller, R.G., Swash, M., Munsat, T.L., 2000. World Federation of Neurology Research Group on Motor Neuron D. El Escorial revisited: revised criteria for the diagnosis of amyotrophic lateral sclerosis. *Amyotrophic lateral sclerosis and other motor neuron disorders : official publication of the World Federation of Neurology*. Research Group on Motor Neuron Diseases 1 (5), 293–299.

Baker, M., Mackenzie, I.R., Pickering-Brown, S.M., et al., 2006. Mutations in progranulin cause tau-negative frontotemporal dementia linked to chromosome 17. Nature 442 (7105), 916–919.

DeJesus-Hernandez, M., Mackenzie, I.R., Boeve, B.F., et al., 2011. Expanded GGGGCC hexanucleotide repeat in noncoding region of C9ORF72 causes chromosome 9p-linked FTD and ALS. Neuron 72 (2), 245–256.

Dale, A.M., Fischl, B., Sereno, M.I., 1999. Cortical surface-based analysis. I. Segmentation and surface reconstruction. *Neuroimage* 9 (2), 179–194.

Desikan, R.S., Segonne, F., Fischl, B., et al., 2006. An automated labeling system for subdividing the human cerebral cortex on MRI scans into gyral based regions of interest. Neuroimage 31 (3), 968–980.

Fischl, B., Salat, D.H., Busa, E., et al., 2002. Whole brain segmentation: automated labeling of neuroanatomical structures in the human brain. Neuron 33 (3), 341–355.

Herholz, K., Adams, R., Kessler, J., Szelies, B., Grond, M., Heiss, W.D., 1990. Criteria for the Diagnosis of Alzheimer's Disease with Positron Emission Tomography. Dement Geriatr Cogn Dis 1, 156–164.

Herholz, K., Salmon, E., Perani, D., et al., 2002. Discrimination between Alzheimer dementia and controls by automated analysis of multicenter FDG PET. Neuroimage 17 (1), 302–316.

Sanabria-Diaz, G., Martinez-Montes, E., Melie-Garcia, L., 2013. Alzheimer's Disease Neuroimaging I. Glucose metabolism during resting state reveals abnormal brain networks organization in the Alzheimer's disease and mild cognitive impairment. PLoS One 8 (7), e68860.

Ihaka, R., Gentleman, R.R., 1996. A Language for Data Analysis and Graphics. J Comput Graph Stat 5, 299–314.

Benjamini, Y., Hochberg, Y., 1995. Controlling the false discovery rate: a practical and powerful approach to multiple testing. Journal of the Royal statistical society: series B (Methodological) 57 (1), 54–70.

N.J. Rutherford M.G. Heckman M. Dejesus-Hernandez et al. Length of normal alleles of C9ORF72 GGGGCC repeat do not influence disease phenotype Neurobiol Aging 33 12 2012 2950 e5–7.

De Vocht, J., Blommaert, J., Devrome, M., et al., 2020. Use of Multimodal Imaging and Clinical Biomarkers in Presymptomatic Carriers of C9orf72 Repeat Expansion. JAMA Neurol.

Mutsaerts, H., Mirza, S.S., Petr, J., et al., 2019. Cerebral perfusion changes in presymptomatic genetic frontotemporal dementia: a GENFI study. Brain 142 (4), 1108–1120.

Bertrand, A., Wen, J., Rinaldi, D., et al., 2018. Early Cognitive, Structural, and Microstructural Changes in Presymptomatic C9orf72 Carriers Younger Than 40 Years. JAMA Neurol 75 (2), 236–245.

Lee, S.E., Sias, A.C., Mandelli, M.L., et al., 2017. Network degeneration and dysfunction in presymptomatic C9ORF72 expansion carriers. NeuroImage Clinical 14, 286–297.

Walhout, R., Schmidt, R., Westeneng, H.J., et al., 2015. Brain morphologic changes in asymptomatic C9orf72 repeat expansion carriers. Neurology 85 (20), 1780–1788.

Boeve, B.F., Boylan, K.B., Graff-Radford, N.R., et al., 2012. Characterization of frontotemporal dementia and/or amyotrophic lateral sclerosis associated with the GGGGCC repeat expansion in C9ORF72. Brain 135 (Pt 3), 765–783.

Cistaro, A., Pagani, M., Montuschi, A., et al., 2014. The metabolic signature of C9ORF72-related ALS: FDG PET comparison with nonmutated patients. European journal of nuclear medicine and molecular imaging 41 (5), 844–852.

Josephs, K.A., Duffy, J.R., Strand, E.A., et al., 2014. Progranulin-associated PiB-negative logopenic primary progressive aphasia. J Neurol 261 (3), 604–614.

Kerklaan, B.J., van Berckel, B.N., Herholz, K., et al., 2014. The added value of 18-fluorodeoxyglucose-positron emission tomography in the diagnosis of the behavioral variant of frontotemporal dementia. Am J Alzheimers Dis Other Demen 29 (7), 607–613.

McDade, E., Boeve, B.F., Burrus, T.M., et al., 2012. Similar clinical and neuroimaging features in monozygotic twin pair with mutation in progranulin. Neurology 78 (16), 1245–1249.

Van Laere, K., Vanhee, A., Verschueren, J., et al., 2014. Value of 18fluorodeoxyglucose-positron-emission tomography in amyotrophic lateral sclerosis: a prospective study. JAMA Neurol 71 (5), 553–561.